Lab on a Chip

PAPER

View Article Online
View Journal | View Issue

Cite this: *Lab Chip*, 2025, **25**, 6718

Microfluidic analysis of salt-stress-mediated antibiotic tolerance in *Mycobacterium smegmatis*

Akanksha Agrawal,[a] Dhananjay Udaya Kumar,[a] Raju Mukherjee†*[a] and Dileep Mampallil †*[b]

Received 18th July 2025,
Accepted 4th November 2025

DOI: 10.1039/d5lc00713e

rsc.li/loc

Understanding how bacteria respond to complex environmental stresses is essential for addressing antibiotic resistance. In the natural environment, bacteria can experience salt stress, for instance, due to spontaneous water evaporation. Here, we present a microfluidic platform that enables long-term culture of *Mycobacterium smegmatis*, a fast-growing, non-pathogenic model for mycobacteria. Using a microfluidic gradient generator, we established stable salt and antibiotic concentration profiles across growth chambers and monitored bacterial proliferation over multiple generations. When exposed to antibiotics in conjunction with elevated salt concentrations, *M. smegmatis* exhibited a significant increase in the minimum inhibitory concentration, indicating a salt-induced drug resistance. Salt stress also led to slower growth, shorter cell length, and reduced division asymmetry. While efflux pump inhibitors partially restored antibiotic sensitivity, gene expression profiles and dye-based efflux assays showed minimal early activation of known efflux genes, but upregulation of ribosomal biosynthesis and stress adaptation. In general, these findings demonstrate how abiotic stress promotes phenotypic drug tolerance and reshapes antibiotic susceptibility prior to developing genetic resistance, thus providing valuable insights into managing the global threat of antibiotic resistance.

1 Introduction

The silent pandemic of antimicrobial resistance (AMR) is an emerging global health threat, driven by the misuse of antibiotics in human medicine, veterinary practices, and agriculture. The rise of resistant bacteria makes infections harder to treat, resulting in prolonged illness, increased medical costs, and higher mortality rates.[1–3] AMR in tuberculosis remains a major concern, accounting for approximately 13% of all AMR-related deaths worldwide.[4] Managing drug-resistant tuberculosis is particularly challenging due to delayed diagnosis and limited access to effective treatment options.[5]

Recent advances in rapid molecular diagnostics and next-generation sequencing have improved the detection and understanding of resistance mechanisms. These mechanisms manifest at three broad levels: genetic resistance, antibiotic tolerance, and persistence,[6–8] highlighting the multifactorial and complex nature of AMR.

Physicochemical factors in the environment can influence bacterial tolerance to antibiotics.[9–12] For instance, human serum has been shown to induce significant antibiotic tolerance in *Staphylococcus aureus*,[13] and pH fluctuations or antibiotic-triggered reactive oxygen species (ROS) contribute to the development of *de novo* resistance.[14,15]

One common physicochemical stressor experienced by bacteria is increased salt concentration, which can occur naturally through evaporation from confined environments such as drops,[16,17] bioaerosols, and soil.[18] Salt stress and confinement have been linked to antibiotic tolerance; for example, mycobacteria pre-cultured in physiological levels of NaCl show elevated minimum inhibitory concentrations (MICs) for various antibiotics. This effect has been attributed to alterations in the plasma membrane and outer membrane lipid composition.[19,20] Salt stress has been shown to protect *Escherichia coli* from antibiotics by inducing efflux pump expression.[10] Similarly, as demonstrated using microfluidics, confinement also induces drug tolerance in *Mycobacterium*, *via* the expression of efflux pumps, a characteristic that is a potential explanation for macrophage-induced drug tolerance.[21] These observations underscore the influence of environmental factors on bacterial susceptibility to antibiotics.

Microfluidic systems provide a powerful platform to study environmental stressors and monitor bacterial responses at high spatial and temporal resolution.[22,23] Various microfluidic

[a] *Department of Biology, Indian Institute of Science Education & Research (IISER), Tirupati 517619, India. E-mail: raju.mukherjee@iisertirupati.ac.in*
[b] *Department of Physics, Indian Institute of Science Education & Research (IISER) Tirupati, India. E-mail: dileep.mampallil@iisertirupati.ac.in*
† The authors contributed equally to this work.

strategies have been developed to study bacterial behavior, offering valuable insights into population heterogeneity at the single-cell level.[24,25] Microfluidics-based studies have played a landmark role in our understanding of the asymmetrical division pattern in *Mycobacterium smegmatis*.[26] Traditional antibiotic susceptibility testing, typically performed in microtiter plates,[27] can be replicated using continuous-flow microfluidic systems with integrated serial dilution.[28] Droplet-based microfluidics has also been applied to investigate bacteria–antibiotic interactions[29,30] and, more recently, to mimic evaporating bioaerosols and assess bacterial (*E. coli*) viability under salt stress.[31] Microfluidic single-cell, high-throughput approaches have advanced our understanding of antibiotic sensitivity and resistance development, including direct visualization of persister cell formation over time.[32,33]

In this study, we examined the growth kinetics and stress responses of *Mycobacterium smegmatis* under salt and antibiotic exposure. *M. smegmatis* is a fast-growing, Gram-positive bacterium commonly used as a non-pathogenic model for *Mycobacterium tuberculosis*. As a saprophytic soil organism, it is frequently exposed to diverse abiotic and biotic stressors in its environment.[34] To counteract growth inhibition caused by antibiotics produced by competing microorganisms, it harbors an extensive repertoire of efflux pumps embedded in its cell membrane.[35–38]

Using a microfluidic discrete gradient generator, we established six different concentrations of salt and antibiotics across growth chambers, allowing *M. smegmatis* to proliferate over multiple generations. Under elevated salt concentrations, the cells exhibited a marked increase in antibiotic MICs, slower growth, reduced cell length, and diminished division asymmetry. Although efflux pump inhibitors partially restored antibiotic sensitivity, RNA sequencing and dye-based efflux assays revealed minimal early activation of known efflux genes after two hours of treatment. Instead, we observed upregulation of stress adaptation genes and certain transcriptional regulators. Our findings offer new insights into how abiotic stress can induce phenotypic drug tolerance and inform future strategies for managing antibiotic resistance.

2 Materials and methods

Bacterial strains and growth conditions

All the reagents for cell culturing were purchased from Sigma unless specified otherwise. The *Mycobacterium smegmatis* MC^2155 strain (wild type) in broth was grown in the Middlebrook 7H9 complete medium (BD Difco) supplemented with 0.2% glycerol, 0.05% Tween-80 at 37 °C under 180 rpm shaking conditions. On the plate, it was grown on Middlebrook 7H10 agar supplemented with 2% glucose at 37 °C. A primary broth culture was inoculated from an isolated colony picked from the plate. For all assays, secondary culture in the mid-logarithmic growth phase (when bacteria are actively dividing) was used. The optical density (OD) measured at 600 nm (OD_{600}) was between 0.5 and 0.8 (OD = 1 implies 1×10^8 cells per ml).

Drug susceptibility assay

The MIC was assessed using a resazurin microtitre assay (REMA) in sterile 96-well round-bottom plates (Costar). The viable cells convert purple colored resazurin to pink colored resorufin. The conversion can be measured by monitoring the fluorescence excitation/emission spectra of 530/590 nm.

MIC values of the respective antibiotics were determined by using a two-fold serial dilution in Middlebrook 7H9 complete media with and without NaCl supplementation (Table 1). The MIC assay was also performed in the presence of efflux pump inhibitors: verapamil (100 μg ml^{-1}) (VER) and thioridazine (10 μg ml^{-1}) (THZ).

Cells were grown to the mid-logarithmic phase ($OD_{600} \approx 0.5$) and serially diluted 1000-fold to $OD_{600} \approx 0.0005$. Each well contained a total volume of 100 μL, comprising 50 μL of antibiotic dilution and 50 μL of diluted bacterial suspension. Positive control wells (cells without antibiotics) and negative control wells (medium only – no cells) were included in each plate.

The plates were incubated at 37 °C for 48 hours under static conditions. Following incubation, resazurin solution was added to each well at a final concentration of 30 μg ml^{-1}. The plates were incubated for an additional 4–6 hours at 37 °C till the color change from purple (resazurin) to pink (resorufin) was observed in the positive well. The fluorescence readings were obtained using a plate reader (Microtek).

RNA sequencing

Mycobacterium smegmatis cells were grown in the 7H9 complete medium till an OD_{600} of 0.5. They were serially diluted to an OD of 0.0005 and were exposed to 250 mM NaCl, $1C_{MIC}$ STR and 250 mM NaCl + $8C_{MIC}$ STR for two hours at 37 "°C. The experiments were carried out with 3 replicates per condition. The control set was untreated *M. smegmatis*. The cells were resuspended in TRIzol, and then homogenized using a bead beater (MPBIO). The cells were vigorously shaken for 10 s with a 30 s cooling on ice for a total of 10 cycles. From the whole cell lysate, phenol:

Table 1 Antibiotics, their classes, concentrations used in the study, and MIC values. All values are presented in their original reported units

Antibiotics	Drug class	Concentration used in this study	MIC (C_{MIC})
Streptomycin (STR)	Aminoglycoside (inhibits protein synthesis)	16–32 000 ng ml^{-1}	250 ng ml^{-1}
Ethambutol (EMB)	Ethanolamine (inhibits cell wall synthesis)	0.06–64 mg ml^{-1}	0.5 mg ml^{-1}
Norfloxacin (NOR)	Fluoroquinolone (inhibits DNA gyrase)	0.5–32 mg ml^{-1}	8 mg ml^{-1} (ref. 39)
Moxifloxacin (MOX)	Fluoroquinolone	12.5–800 mg ml^{-1}	50 mg ml^{-1} (ref. 39)

chloroform-based RNA extraction was carried out. The RNA was cleaned using the RNeasy kit (Qiagen). The library prep was carried out using the QIAseq Stranded RNA Library kit. The resultant library was subjected to Illumina (Novaseq 6000) sequencing.

Transcriptome analysis

The raw FASTQ reads were preprocessed using Fastp v.0.23.4.[40] The trimmed fastp reads were aligned against the SILVA database to filter the rRNA reads using Bowtie2 (ref. 41) v2.4.5. The reference genome used for *Mycobacterium smegmatis* (GCF_000015005.1) was indexed using Bowtie2 v2.4.5. The rRNA filtered reads were mapped to the indexed reference genome using STAR[42] v2.4.5. The BAM files from individual samples were quantified using featureCounts v. 2.0.1 (ref. 43) based on the filtered GTF file to obtain gene counts. These gene counts for *Mycobacterium smegmatis* were used as inputs in the R package DESeq2 (ref. 44) for differential expression estimation (parameters: threshold of statistical significance – alpha 0.05; the *p*-value adjustment method: Benjamini–Hochberg). The DESeq2 result files were filtered based on the adjusted *p*-value (FDR) $\leqq 0.05$ and Log_2-FoldChange $\pm$ 1 that were used as cut-offs to filter the significant genes.

Microfluidic device

The microfluidic device comprises two main regions: (i) a discrete gradient generation region and (ii) a cell growth region. The gradient generator is designed to create six distinct final concentrations from the two input concentrations introduced at the inlets. This region contains channels that are 30 μm high and 100 μm wide. To enhance mixing efficiency, 30 μm × 30 μm indentations were introduced along the channels at 90 μm intervals, giving the channels a serrated appearance (Fig. 1). The cell growth region consists of triangular wave-shaped channels. To retain cells within these channels and prevent them from being flushed away, the channel height in this region was reduced to 4 μm, allowing the monolayer growth of *M. smegmatis* cells, allowing clear observation of the individual cells.

The channel design was micro-patterned onto a silicon wafer in two steps. First, the cell growth region was molded onto the wafer using a SU8-3005 photoresist at a height of 4 μm. The patterning was performed with a maskless lithography system (Microlight 3D – Smart Print). Next, on the same wafer, the mixing region was molded using the Ordyl SY300 dry photoresist (Resistechno) at a height of 30 μm. Here, the dry film was gently placed onto the silicon wafer after depositing a few drops of water on the wafer to prevent the film from wrinkling. The water between the film and the wafer was removed by gently wiping spirally outward with a Kimwipe tissue. The patterning of the dry film was performed with the maskless lithography system. The exposure energy and baking protocols were obtained from the respective photoresist datasheet.

Channels were fabricated by soft lithography using a silicon wafer mold. A mixture of polydimethylsiloxane (PDMS; SYLGARD 184, Dow Corning) and the curing agent in a 10 : 1 (v/v) ratio was poured onto the micro-patterned wafer and cured at 70 °C for 60 minutes. The cured PDMS replica was then bonded to a glass cover slip (Corning) that had been cleaned by sonication in a 1 : 1 (v/v) solution of acetone and isopropanol. Prior to bonding, both the PDMS surface and the glass cover slip were treated with oxygen plasma (Diener Electronic Zepto) for 40 seconds to facilitate permanent bonding. Enhanced mixing in the serrated channels, though modest, was clearly observable in a simple food-color-based experiment compared to the unserrated channels (Fig. S1).

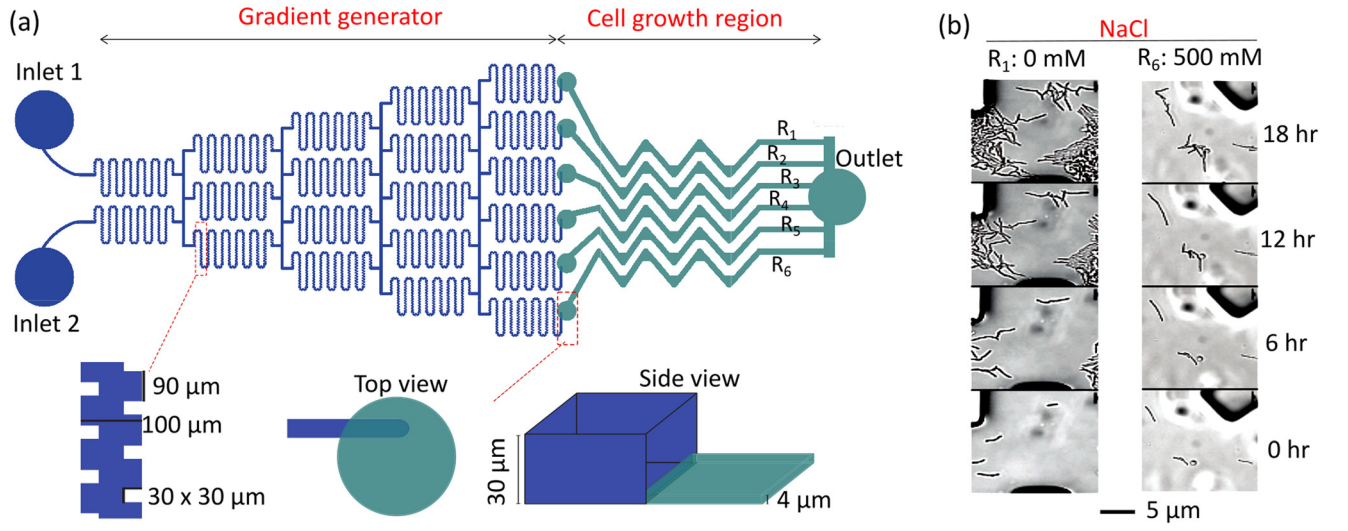

Fig. 1 (a) Schematic of the microfluidic device. Fluids from the two inlets are mixed in the gradient-generating region, producing six distinct salt/drug concentrations across the cell growth regions R_1 to R_6. The serrated channels improved mixing (Fig. S1). (b) Representative growth patterns of *M. smegmatis* when inlet 1 received the medium with 0 mM NaCl and inlet 2 with 500 mM NaCl.

Microfluidics experiments

EVOS M7000 with a stage top incubator was used for all the microfluidics-based experiments. The temperature was maintained at 37 °C. A 100× oil immersion (Olympus) objective was used for imaging. The multiple-point time-lapse imaging was performed with the autofocus enabled, unless specified otherwise.

Growth curve. The device was initially infused with the 7H9 complete medium through both inlets to prime the channels. Following this, the media flow was paused, and mCherry (a red fluorescent protein) expressing *M. smegmatis* cells were introduced into the cell growth region *via* the outlet channel. After cell loading, the outlet was connected to a waste container. The entire device was then placed on a stage-top incubator mounted on an inverted fluorescence microscope (EVOS M7000), where the temperature was maintained at 37 °C. Continuous flow of the 7H9 complete medium was resumed through both inlets at a rate of 2.5 μl min^{-1} using a syringe pump (Harvard apparatus 11 Elite). This small flow rate maintained a nutrient supply, however, without drifting the cells out of the channels.

Cell growth was monitored by measuring the growth rate at five randomly selected locations within each cell growth region. The cells were imaged at 20-minute intervals for a period of 24 hours.

To measure the growth curve at different NaCl concentrations, a salt gradient was established by supplying 7H9 complete media and media supplemented with 500 mM NaCl through the two inlets. This generated final NaCl concentrations of c_0 + [0, 100, 200, 300, 400, and 500] mM across the six cell growth channels, where c_0 represents the background NaCl concentration in the 7H9 complete medium.

To measure the growth curve at different streptomycin (STR) concentrations, the 7H9 complete medium was supplied through the two inlets—one without STR and the other supplemented with $5C_{MIC}$ STR, where C_{MIC} = 250 ng ml^{-1}. This setup generated STR concentrations of $0C_{MIC}$, $1C_{MIC}$, $2C_{MIC}$, $3C_{MIC}$, $4C_{MIC}$, and $5C_{MIC}$ across the six cell growth channels. In a separate set of experiments, STR was maintained at $2C_{MIC}$ in all channels while a NaCl gradient was established to study the combined effect of salt and antibiotic stress.

Calcein-AM uptake and efflux assay. To measure the uptake, actively growing wild-type *M. smegmatis* cells were introduced into a microfluidic device. The cells were infused with 7H9 complete media supplemented with 2 μM Calcein-AM Violet (CAM) (Invitrogen, Thermo Fisher) at a flow rate of 2.5 μl min^{-1} using a syringe pump. Uptake studies were conducted at 37 °C, with reagents supplied through the media.

To measure efflux, actively growing *M. smegmatis* cells were treated with Calcein-AM Violet at a final concentration of 2 μM in a 1 ml volume. The cells were incubated with the dye for 30 minutes at 37 °C, washed with fresh 7H9 complete media, and introduced into the microfluidic device.

The CAM uptake and efflux were captured at the excitation/emission spectra of 400 nm and 452 nm, respectively. The images were taken at a 2-minute interval for a period of two hours in each experiment. The focus was manually adjusted prior to each timepoint before imaging.

In all the microfluidic experiments, 7H9 complete media were infused into the device at a flow rate of 2.5 μl min^{-1}. Under each experimental condition, at least 100 cells were monitored.

Image analysis. Using ImageJ FIJI, a time-lapse video was compiled using the best *z*-plane per timepoint. The *xy*-plane drift correction was performed using ImageJ plugin: Fast4DReg.[45] In ImageJ, ROI containing a bacterial colony was cropped for further analysis. In the program Cell-ACDC,[46] *Msmeg* cells were identified using the Omnipose-Bacphase[47] segmentation module. The Excel file obtained as a result was compiled to obtain the generation time, parent cell length (D_{Parent}), and daughter cell lengths, which were further used for the calculation of the ratio of the daughter cells (D_1/D_2).

Statistics. Graph preparation and statistical analyses were conducted using Prism v9.5.1 (GraphPad). Differences between the groups were evaluated using two-way analysis of variance (ANOVA). Statistical significance was defined by the following *P* values: *, $P < 0.05$; **, $P < 0.01$; ***$P < 0.001$, and ****, $P \leq 0.0001$.

3 Results and discussion

3.1 Salt stress response in the bulk

We started with testing the salt tolerance of *M. smegmatis* in the bulk for preliminary observation. We grew the bacteria for 6 h in the presence of NaCl with concentrations ranging from 0 to 1000 mM. Our bulk assays showed no significant reduction in its viability until 500 mM NaCl. However, at 1000 mM NaCl, we observed a reduction in the number of colonies (Fig. S2).

Observing that 500 mM salt was not lethal to *M. smegmatis*, we monitored its growth at 250 mM and 500 mM salt. We observed that the generation time for cells grown in 250 mM NaCl was similar to that of the untreated culture. However, a prolonged initial growth phase (often called the lag phase) was observed for the cells grown in 500 mM NaCl with a concomitant increase in their generation time from 3 h to 5 h (Fig. S3).

M. smegmatis growth remains unaffected at least up to 500 mM, indicating that the bacterium is capable of mounting an adaptive response to moderate salt stress. These internal changes may also influence bacterial drug tolerance.

Comparative studies in soil bacteria reveal NaCl-dose-dependent inhibition of growth. The salt concentration leads to reduced enzyme activity affecting processes like respiration and biomass synthesis, prolonging the generation time as cells prioritize survival over proliferation.[48,49]

To check the correlation between exposure to salt and drug tolerance, we measured the susceptibility of the salt-stressed bacteria to different classes of antimycobacterial drugs (Table 1), such as streptomycin (STR), ethambutol (EMB),

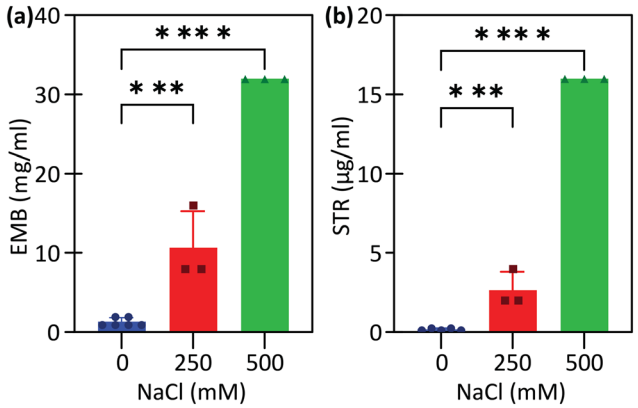

Fig. 2 The MIC in *M. smegmatis* at different NaCl concentrations in the bulk culture. When cultured with salt, the MIC increased in a dose-dependent manner for the tested antibiotics: (a) ethambutol (EMB) and (b) streptomycin (STR). Under standard conditions, the MIC for EMB and STR is 0.5 mg ml^{-1} and 250 ng ml^{-1}, respectively. Data represent mean ± SD of three independent experiments (individual data points are marked on the bars). Error bars are too small for the case of 500 mM.

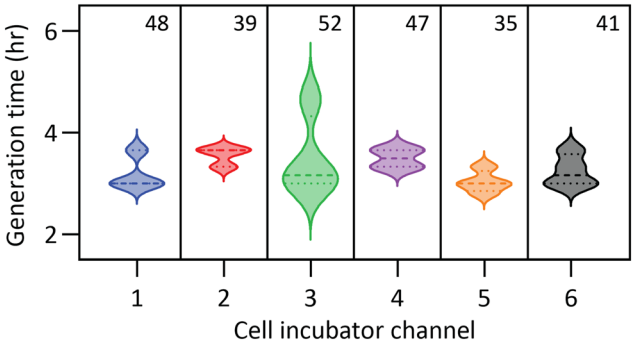

Fig. 3 Growth of *M. smegmatis* inside a microfluidic device. The generation time was found to be similar in all six channels (R_1–R_6 in Fig. 1), indicating similar conditions. In this reference measurement, the input was 7H9 complete media from both inlets without any added salt. The number of cells monitored in each channel is mentioned in the panel.

moxifloxacin (MOX), and norfloxacin (NOR). In the presence of 250 mM and 500 mM NaCl, we observed that the MIC for STR, EMB (Fig. 2), and NOR increases (Fig. S4). There was no noticeable change in the MIC for MOX with salt (Fig. S4).

Previously, in mycobacteria, both short- and long-term pre-exposure to elevated NaCl concentrations have been shown to induce drug tolerance[19,20]—a phenomenon in which a substantial subpopulation of cells partially resists the action of high antibiotic concentrations, leading to delayed cell death. Interestingly, we did not observe any noticeable effect from pre-exposure, but only from co-culture with salt. The mycobacterial outer membrane is rich in lipids, and this feature differentiates the permeability and uptake of small molecules. While hydrophilic molecules like nutrients may use a porin-mediated uptake, the permeability of the hydrophobic molecules through passive diffusion depends on their lipophilicity. The absence of the effect of salt in the case of moxifloxacin may be linked to its hydrophilic nature ($\log P$ of 1.47) compared to the lipophilic fluoroquinolone, norfloxacin ($\log P$ of 0.01–0.96).

3.2 Confirming bacterial growth inside the microfluidic device

While bulk culture experiments allow measurement of average physiological parameters and the plotting of growth curves based on the culture viability count, they do not capture the physiological and morphological heterogeneity within bacterial populations, such as variations in cell length or daughter cell size over time. To address this limitation, we performed measurements in the microfluidic channel.

To ensure the viability of the cells inside the device, we first investigated the growth of *M. smegmatis* in the microfluidic device and quantified the growth rate.

Cells were continuously supplied with the 7H9 complete medium through both inlet tubes at a flow rate of 2.5 μl min^{-1}. Under these conditions, *M. smegmatis* exhibited an average generation time of 3 hours, as determined from three independent measurements. This generation time was consistent across all parallel channels of the cell growth region, ensuring that any observed phenotypic differences could be attributed solely to the applied gradient treatment. Any variation in the growth rate across micro-colonies, as shown in Fig. 3, highlights the intrinsic heterogeneity in *M. smegmatis* growth, features that are often masked in bulk culture assays.

3.3 Bacterial growth inside the microfluidic device with salt alone

After confirming the normal growth of *M. smegmatis* within the microfluidic device, we established NaCl concentrations of 0, 100, 200, 300, 400, and 500 mM by supplementing the culture medium entering one inlet with an additional 500 mM NaCl. While maintaining the device inside a stage-top incubator, we monitored the cell growth. Increased salt (>300 mM) showed decreased cell replication (Fig. S5 and Video S1).

The elongation rate of individual cells prior to division was recorded for multiple generations (Fig. 4). From these data, the generation time, the length of the parent cell just before division, and the ratio of the shorter to longer daughter cells were quantified across the different salt concentrations, as presented in the histograms in Fig. 5.

We observed that the generation time of *M. smegmatis* increases from 3 h in untreated conditions to 5–8 h in 500 mM NaCl (Fig. 5A). This result is consistent with that from the bulk cultures (Fig. S3).

The substantial increase in generation time is associated with the bacterial response to hyperosmotic stress. Studies in *E. coli* have shown that adaptation to such stress involves a multi-step process, beginning with the rapid upregulation of K^+ uptake systems, followed by the synthesis of osmo-protective molecules such as trehalose.[49] *E. coli*, confined in evaporating microfluidic emulsion droplets,[50] also demonstrated K^+

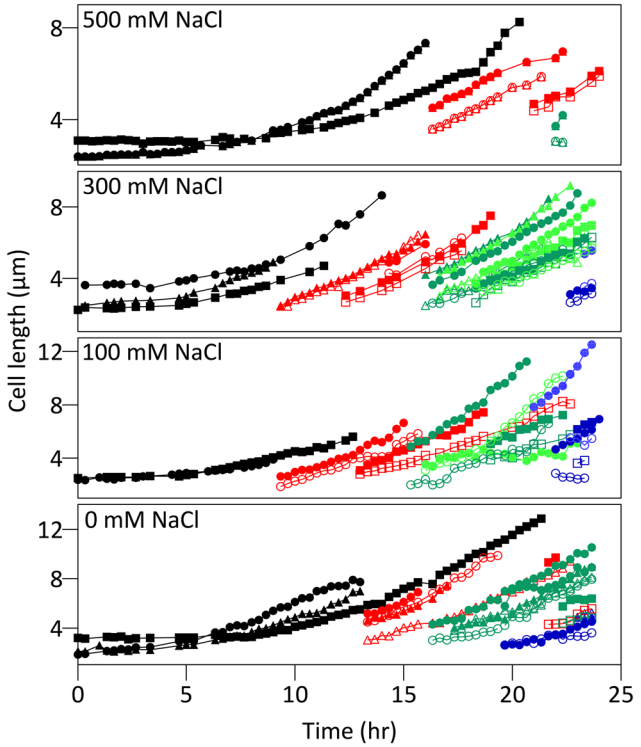

Fig. 4 Time course data where the cell length of *M. smegmatis* was monitored inside the device over multiple generations at different NaCl concentrations. Curve colors – black, red, green, and blue – indicate successive generations. The symbol type denotes the same lineage, while open and filled symbols represent the alternator and accelerator daughter cells, respectively.

uptake.[31] In addition, osmotic stress can trigger remodeling of the cell envelope, as observed in *Mycobacterium* species.[19,20]

We observed that under untreated conditions, the average parent cell length was 6.7 ± 2 μm. As the NaCl concentration increased, this length gradually decreased, reaching 5.5 ± 1.7 μm at 500 mM NaCl (Fig. 5A).

M. smegmatis is known to undergo asymmetric cell division,[26,51] producing two daughter cells of unequal length. The shorter cell, referred to as the alternator, exhibits slower growth, while the longer cell, known as the accelerator, grows at a relatively faster rate. In this study, the division asymmetry is quantified as the ratio of the alternator to the accelerator cell length (D_1/D_2). We observed that while untreated cells exhibited ratios clustered between 0.5 and 0.8, this range shifted to 0.8 and 1.0 under 500 mM NaCl. It indicates that salt treatment promotes more symmetric division in *M. smegmatis*.

3.4 Effect of antibiotic treatment on bacterial growth and morphology

We first examined the effect of streptomycin (STR) alone (without added salt) on *M. smegmatis*. STR concentrations were generated in the microfluidic device by supplying the 7H9 complete medium without STR through one inlet and with $5C_{MIC}$ STR through the other. This setup produced final STR concentrations of $0C_{MIC}$, $1C_{MIC}$, $2C_{MIC}$, $3C_{MIC}$, $4C_{MIC}$, and $5C_{MIC}$ across the cell culture region. As expected, the cells exposed to $1C_{MIC}$–$5C_{MIC}$ STR showed progressive cell death, with the highest concentration leading to more rapid killing (Fig. S6 and Video S2). Morphological changes were also observed, with cells losing their characteristic rod shape under STR treatment. Notably, replacing the antibiotic with fresh 7H9 medium did not lead to resuscitation, indicating that the cells had undergone irreversible death. Similar morphological changes have been reported for EMB and isoniazid, where the cells from different *Mycobacterium* species became shorter and more rounded.[52–54] In the case of *Mycobacterium abscessus* subjected to up to a 16-fold MBC (minimum bactericidal concentration) for MOXI, the resultant persister cells showed heterogeneity in the cell shape, where reduced-sized, ovoid-shaped, and cell wall-deficient-shaped cells were also observed.[55]

To evaluate the impact of co-treatment with salt and antibiotics, $2C_{MIC}$ STR was maintained throughout the device while generating a NaCl gradient of 0, 100, …, 500 mM. Consistent with the STR-only treatment, cells in the 0 mM NaCl channel exhibited cell death. The growth rate was slow with increasing salt (Fig. S7). Interestingly, the cells exposed to 100–500 mM NaCl survived and retained a normal cellular morphology. The parent cell length and the daughter cell length ratio followed the same trend observed under NaCl gradient conditions alone, as shown in Fig. 5B and S7.

It is known that drug exposure induces a reduction in growth rates and metabolic shift in *Mycobacterium*.[56,57] Microfluidic single-cell studies have shown irreversible reduction in intracellular ATP levels in *Mycobacterium* upon exposure to antibiotics.[57] Also, single-cell studies reveal that preexisting variations in DNA damage response correlates with heterogeneous susceptibility to fluoroquinolones in *Mycobacterium*.[58] Increasing NaCl concentrations in the growth medium impose osmotic stress on bacterial cells. Osmoprotectant molecules such as trehalose help mitigate this stress. However, even at high NaCl concentrations, disruption of trehalose-containing complexes such as trehalose monomycolate and trehalose dimycolate – which are essential components of the mycobacterial cell envelope – has not been shown to confer drug resistance.[19] Alterations in trehalose metabolism, however, have been associated with the promotion of drug tolerance, a transient phenotypic state that may serve as a precursor to the eventual development of stable, genetically encoded antibiotic resistance.[59] Another phenotypic mechanism of drug tolerance involves the activity of efflux pumps,[60] yet the potential influence of NaCl on efflux pump expression in *Mycobacterium* remains largely unexplored.

3.5 Efflux pump inhibitors partially rescue drug sensitivity under STR + NaCl co-treatment

In drug resistance, cell envelope-bound pumps efflux out antibiotics from the cells. To assess whether efflux pumps contribute to the substantial increase in the MIC, rising from

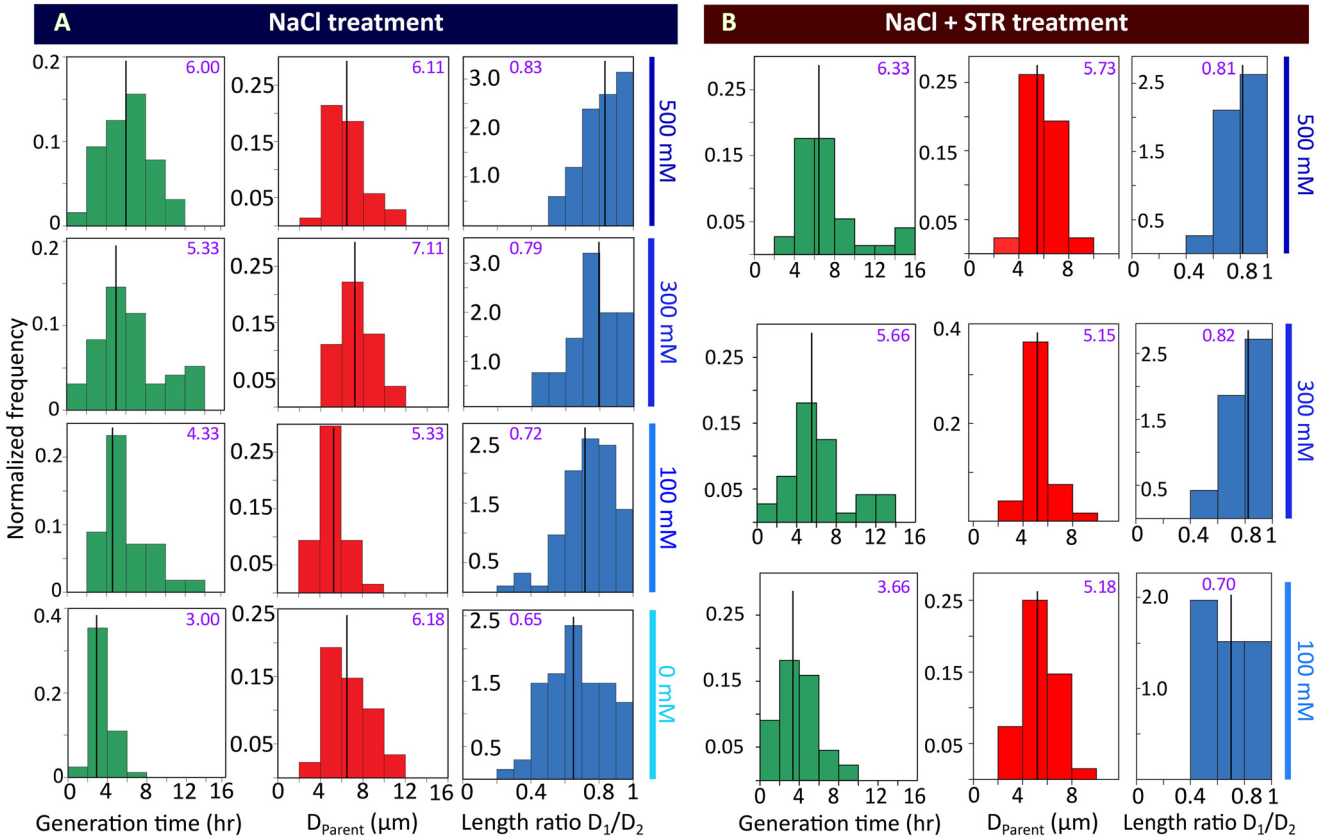

Fig. 5 Growth parameters of *M. smegmatis* in the device at different (A) NaCl and (B) NaCl + 2C_{MIC} STR concentrations. Histograms of the generation time, parent cell length just before division (D_{Parent}), and length ratio of daughter cells (D_1/D_2) are plotted. (A): The generation time increases and D_{Parent} decreases with increasing [NaCl]. D_1 and D_2 are the lengths of the shorter and longer daughter cells, respectively, measured soon after the division. (B): With NaCl + 2C_{MIC} STR, the growth parameters show a similar trend as in the case of NaCl alone. At 0 mM NaCl, the cells died at 2C_{MIC} STR. The presence of NaCl provides conditioning against STR. The data points per plot were collected from 3 independent experiments involving a total of 103 cell divisions. The median value is written and marked by a single black line in each panel.

250 ng ml^{-1} to 4 μg ml^{-1} and 16 μg ml^{-1} in the presence of 250 mM and 500 mM NaCl, respectively, we performed drug sensitivity assays with efflux pump inhibitors in the 96-well plates. If efflux activity mediated the resistance under high-salt conditions, we expect a reduction in the MIC upon inhibitor treatment. We used two well-established inhibitors, verapamil (VER) and thioridazine (THZ). Verapamil has been shown to inhibit energy-dependent efflux activity in *Mycobacterium tuberculosis*, enhancing antibiotic efficacy.[61] Similarly, thioridazine has demonstrated efflux inhibitory activity and potential as an adjuvant in TB therapy.[62]

Co-administration of VER or THZ with antibiotic STR lowered the MIC below the baseline value observed under no-salt conditions (Fig. 6 conditions, a–c). Under co-treatment with STR + 500 mM NaCl, the elevated MIC of 16 μg ml^{-1} decreased to 4 μg ml^{-1} when either inhibitor was added (Fig. 6 conditions, e and f). While 4 μg ml^{-1} remains 16-fold higher than the untreated MIC (Fig. 6 condition, a), it represents a 4-fold reduction compared to the STR + NaCl condition without inhibitors (Fig. 6 condition, d).

The partial reversal of the elevated MIC by efflux pump inhibitors suggests that efflux pump activity contributes to the increased MIC observed under NaCl-induced osmotic stress. This is consistent with previous findings showing that efflux systems are upregulated in response to stress. For instance, exposure to the stressful intracellular environment of macrophages has been shown to induce efflux pump expression in *M. tuberculosis*.[60]

3.6 Drug uptake and efflux in the presence of salt stress

Upon observing that efflux pump inhibitors partially restored STR sensitivity, we directly measured the efflux pump activity at early time points following exposure to NaCl and STR in the device. To assess this, we utilized Calcein-AM Violet (CAM), a non-fluorescent ester dye that passively diffuses into cells and is hydrolyzed by intracellular esterase to yield a fluorescent calcein derivative. In the absence of active efflux, this fluorescent derivative accumulates within the cell, making CAM a widely used probe for monitoring efflux activity in both bacterial and mammalian systems.[63,64]

First, we monitored the diffusion of CAM into the cells. Infusing 7H9 complete media with 2.5 μM CAM-Violet, the fluorescence saturation of the cells was reached in 10 minutes. However, when the media were supplemented with an additional 500 mM NaCl, the saturation of the dye was

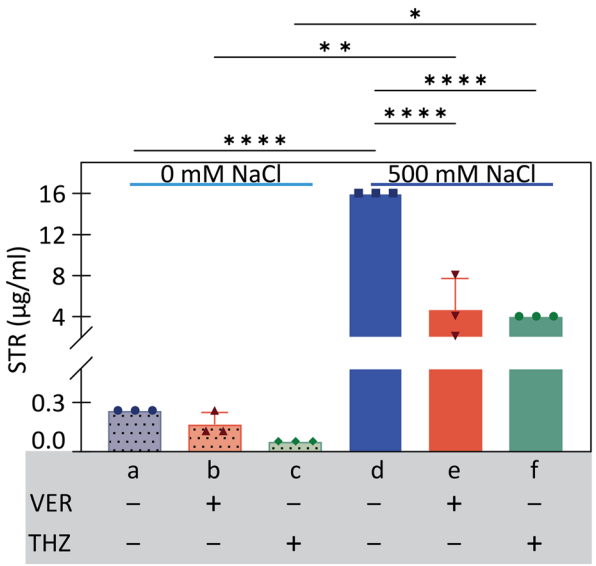

Fig. 6 Efflux pump inhibitors partially rescue antibiotic sensitivity. The MIC was measured at the end of 48 hours after the respective treatment conditions. VER (100 μg ml^{-1}) and THZ (10 μg ml^{-1}) bring down the MIC when added to the antibiotic plates. During co-treatment with 500 mM NaCl, the STR MIC increases to 16 μg ml^{-1} from 0.25 μg ml^{-1}. VER and THZ bring down the MIC to 4 μg ml^{-1}, resulting in the partial rescue of STR sensitivity. Each condition with VER and THZ added (+) or not added (–) is labeled from (a) to (f). Data represent mean ± SD of three independent experiments. Error bars are too small for a, c, d, and f.

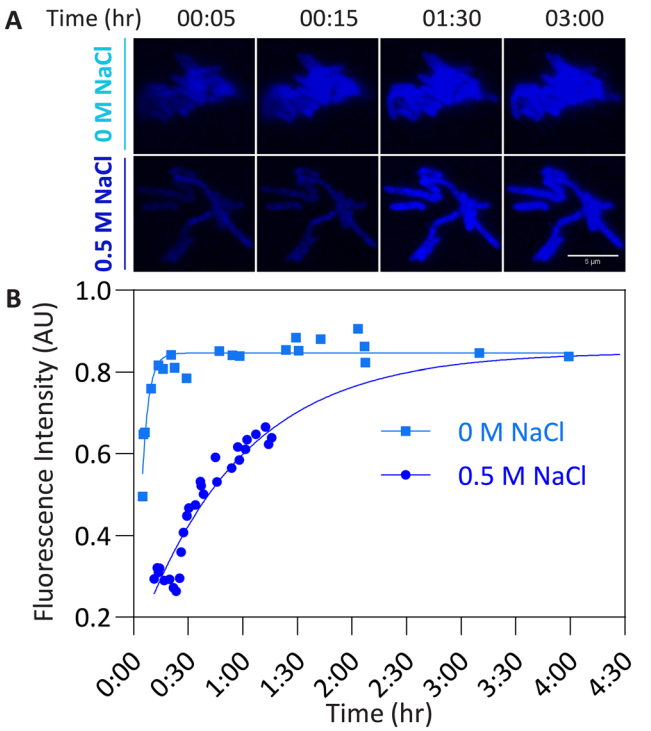

Fig. 7 (A) Time-lapse images of CAM-violet uptake by *M. smegmatis* treated with an additional 0 and 500 mM NaCl. Scale bar represents 5 μm in each frame. (B) Calcein AM uptake is slower in the presence of elevated salt compared to the reference condition, hinting that diffusion of small molecules (say, antibiotics) into the cells is diminished soon after the salt stress. The fluorescence intensity was normalized for individual time lapse data using the formula: $(I(t) - I_{min})/(I_{max} - I_{min})$, where I_{min} and I_{max} are the lowest and highest intensity values of the cells in the time-lapse data.

reached only after 2 h, as shown in Fig. 7. These findings suggest that elevated NaCl concentrations hinder the diffusion of molecules like CAM—and possibly antibiotics. While drug susceptibility assays were conducted after 48 hours of growth, CAM uptake measurements indicate that the reduction in small molecule diffusion occurs within 2 hours of NaCl exposure. It could be due to the changes occurring in the cell envelope under Ser/Thr kinase signaling mediated under NaCl-induced osmotic stress, as described previously in *M. tuberculosis*.[20] Another possible reason for the reduced uptake of the cell wall permeable lipophilic calcein (CAM) could suggest a change in the lipid content of the mycomembrane that reduces permeability of lipophilic small molecules, which do not depend on porins for uptake. This also explains the reduced uptake of the lipophilic fluoroquinolone norfloxacin in the presence of 500 mM NaCl. Similarly, confinement has been shown to induce drug tolerance in *Mycobacterium* through the activation of efflux pump mechanisms.[21]

Secondly, we monitored the efflux of the CAM molecules out of the cells. The *M. smegmatis* cells, pre-stained with CAM, were monitored for two hours. We expect a reduction in the fluorescence intensity if the CAM molecules are effluxed. Only a slight reduction in the fluorescence intensity was observed over the two-hour period under NaCl treatment. No significant change in the intensity was observed in the presence of STR, STR + salt, or VER compared to the untreated cells (Fig. S8). These results indicate that efflux activity was not substantially induced by NaCl or STR, at least in the initial two hours. A longer duration was not tested as the cell division itself reduces the intracellular dye concentration.

3.7 Gene expression under short-term NaCl treatment

We performed RNA sequencing to understand the mRNA profile present in the cells under salt stress. We compared the gene expression of cells treated with the three different conditions: (i) 250 mM NaCl, (ii) $1C_{MIC}$ STR, and (iii) 250 mM NaCl + $8C_{MIC}$ STR, for 2 h, against the gene expression in the reference (untreated cells).

We used only salt (250 mM NaCl) and streptomycin ($1C_{MIC}$) as controls to analyze the change in gene expression upon exposure to both salt and the antibiotic (250 mM NaCl + STR). The 250 mM NaCl condition exhibited delayed growth with an extended lag phase; however, the growth rate was comparable to that of untreated cells. Therefore, this concentration was chosen for both the control and the combined treatment with the antibiotic. An inhibitory concentration of streptomycin ($1C_{MIC}$) was used for a short exposure period (2 h), sufficient to induce changes in gene expression without significant loss of viable cells. Since the

minimum inhibitory concentration (MIC) of streptomycin increased from 1 to $16C_{MIC}$ in the presence of salt, we opted to use a sub-inhibitory concentration of $8C_{MIC}$ for the co-treatment condition. Cell viability under these conditions was verified prior to selecting the final concentrations and treatment duration (Fig. S9).

The RNA profiling of our samples revealed widespread and significant changes in gene expression, with numerous genes showing consistent upregulation or downregulation across all treatments. The major ones are listed in Table 2, and the complete list is provided in the SI.

In short, STR-specific markers like *WhiB1,7* were upregulated. Several genes related to ribosomal biosynthesis, such as *rps(H,J,O,P,R,T)*, *rpl(C,M,N,O,S,U,X)*, and *rpm(B,I,J)* were upregulated by 1-fold. Since streptomycin inhibits translation by targeting ribosomal subunits,[66] the observed increase in the expression of ribosomal protein genes may reflect a compensatory response to maintain protein synthesis under antibiotic stress.

While drug exposure tends to induce efflux pump mechanisms,[56,67,68] we did not see any significant change in the known efflux pump genes after two hours of treatment. Nevertheless, in response to STR treatment, we observed a 1-fold upregulation of the putative efflux protein *MSMEG_3670*, which is a probable multidrug efflux SMR (small multidrug resistance) transporter. Notably, we were able to capture the downregulation of a known porin *mspA* (*MSMEG_0965*), which has a probable role in drug (STR) uptake.[65]

Under the 250 mM NaCl-treated samples, we were able to capture the upregulation of genes that have a probable regulatory function, like *MSMEG_5388* and *MSMEG_3129*. Conserved hypothetical genes having transmembrane domains were also upregulated, suggesting modifications in the cell envelope.

During the STR–NaCl co-treatment conditions, among the most strongly upregulated genes were those involved in stress adaptation. Several transposase-encoding genes were also upregulated, including *MSMEG_2821* and *MSMEG_3510*, exhibiting a 2.7- to 3.3-fold increase in all three treatment conditions.

We also found the upregulation of certain conserved hypothetical genes, which have a possible regulatory function. Among the genes downregulated, we were particularly interested in *MSMEG_2303*, as the gene product has a structural homology with an antiporter, important in maintaining the membrane potential in the bacteria. This gene was downregulated by −4-fold under NaCl treatment and by −6.8-fold under the co-treatment conditions. Such downregulation of membrane-bound proteins could affect the membrane potential, essential for the STR uptake.

A pronounced downregulation was observed under all three treatment conditions in genes central to core metabolism, such as *MSMEG_2313*, which codes for the protein 'nrdF2'. It showed changes between −9.43 and −6.39. The protein coded by *MSMEG_2313* is involved in the DNA replication process, functioning in the biosynthesis of deoxyribonucleotides (dNTPs). This downregulation is consistent with the extended lag phase observed when the cells were cultured in 250 mM NaCl.[69] Unlike the other two conditions, under STR treatment, many oxidoreductases and transporters were downregulated (Table 2). In short, we observed upregulation of genes associated with ribosomal biosynthesis, transposase activity, and gene regulation. In contrast, several genes involved in core metabolic pathways were downregulated.

We expected to see the upregulation of efflux pump genes, given that efflux pump inhibitors reduced the MIC during long-term (48-hour) plate assays. However, the transcriptional response did not show strong activation of these genes after the 2-hour treatment. Supportively, our Calcein AM efflux assay in the device, upon 2 hours of treatment with $2C_{MIC}$ STR, showed no significant efflux of the dye *vs.* the untreated control. It implies that efflux did not occur at least in the first 2 hours.

Table 2 Summary of major gene expression changes under different treatment conditions: (i) 250 mM NaCl, (ii) $1C_{MIC}$ STR, and (iii) 250 mM NaCl + $8C_{MIC}$ STR, applied for 2 hours. The upregulation and downregulation were with respect to the reference sample

Gene	$\log_2$ fold change (treatment conditions)	Description
WhiB1	Upregulation (ii)	Expressed under nitric oxide stress
WhiB7	Downregulation (i) Upregulation (ii)	Expression leads to resistance against aminoglycosides (STR)
rps(H,J,O,P,R,T), *rpl(C,M,N,O,S,U,X)*, and *rpm(B,I,J)*	Upregulation (ii)	Related to ribosomal biosynthesis
MSMEG_3670	Upregulation (ii)	Putative efflux protein, a probable multidrug efflux SMR (small multidrug resistance) transporter
MSMEG_5388 and *MSMEG_3129*	Upregulation (i)	Regulatory function
MSMEG_2821 and *MSMEG_3510*	Upregulation (i), (ii) and (iii)	Transposase-encoding genes
MSMEG_0965	Downregulation (ii)	Porin *mspA*, which has a probable role in drug (STR) uptake[65]
MSMEG_1009 and *MSMEG_1008*	Downregulation (i)	Involved in electron transfer like cytochrome p450
MSMEG_2303	Downregulated (i) and (iii)	Important in maintaining the membrane potential in the bacteria
MSMEG_2313	Downregulated (i), (ii) and (iii)	Codes for the protein 'nrdF2'. Function in the biosynthesis of deoxyribonucleotides (dNTPs)

In future studies, the upregulated genes can be cloned to test whether their overexpression confers antibiotic resistance. This would provide insight into the genetic pathways through which salt stress induces resistance.

4 Conclusion

In summary, we present a microfluidics-based investigation of how *Mycobacterium smegmatis* responds to combined salt and antibiotic stress at the single-cell level. Our custom-designed microfluidic device enabled long-term observation of bacterial growth, morphology, and antibiotic susceptibility across spatially distinct salt and antibiotic concentrations.

In the bulk measurements, we found that elevated NaCl concentrations increase the minimum inhibitory concentration (MIC) of several antibiotics, including streptomycin (STR), ethambutol (EMB), and norfloxacin (NOR), indicating that osmotic stress induces a transient drug-tolerant state.

We used a microfluidic system to test single-cell level responses to the exposure to increased salt and antibiotics (STR). Microfluidic experiments enabled us to probe the morphological analyses of the cells. Under salt stress, the cells exhibited slower growth, reduced cell length, and decreased division asymmetry. Calcein AM uptake measurements further revealed that salt stress impairs the diffusion of small molecules into the cells, which may have implications for the elevated MIC observed under such conditions.

Although the use of efflux pump inhibitors (verapamil and thioridazine) partially reversed salt-induced antibiotic tolerance, early transcriptional responses did not reveal strong upregulation of efflux pump genes. Instead, we observed the upregulation of genes involved in ribosomal biosynthesis, stress adaptation, and transposase activity. A putative SMR-family efflux gene (*MSMEG_3670*) was modestly induced under STR treatment. Several core metabolic genes were downregulated, supporting a shift toward a low-activity, tolerant phenotype.

Mycobacteria have evolved to survive multiple stressors *en route* as they get airborne in droplets, during their interhost transit. Salts, such as NaCl, have been reported to provide maximum protection against desiccation.[70] Our work highlights the power of microfluidics in dissecting microbial heterogeneity under combined environmental and pharmacological stress. These findings underscore the need to consider environmental factors like osmotic stress in the evaluation of antimicrobial resistance and suggest that stress-induced tolerance may precede and facilitate the development of genetic resistance. Our results are important for therapeutic intervention and forming future strategies for managing antibiotic drug resistance.

Author contributions

AA, RM, and DM designed the project. AA performed the experiments and analyses. DUK helped with image analysis. DM and RM supervised the project. AA, DM, and RM wrote the manuscript.

Conflicts of interest

There are no conflicts to declare.

Data availability

The data supporting this article have been included as part of the supplementary information (SI).

Supplementary information is available. See DOI: https://doi.org/10.1039/d5lc00713e.

Acknowledgements

The authors would like to acknowledge Rakesh DH, Dishari Biswas, Malavika M Nair, Soumya Nagalikar, Kumar Abhinandan, and Varshini H. for helping with image analyses. DM and RM acknowledge the grant CRG/2020/003117 from the Science and Engineering Research Board (India).

Notes and references

1 E. Cella, M. Giovanetti, F. Benedetti, F. Scarpa, C. Johnston, A. Borsetti, G. Ceccarelli, T. Azarian, D. Zella and M. Ciccozzi, *Pathogens*, 2023, **12**, 1074.
2 B. Aslam, W. Wang, M. I. Arshad, M. Khurshid, S. Muzammil, M. H. Rasool, M. A. Nisar, R. F. Alvi, M. A. Aslam and M. U. Qamar, *et al.*, *Infect. Drug Resist.*, 2018, 1645–1658.
3 F. Prestinaci, P. Pezzotti and A. Pantosti, *Pathog. Global Health*, 2015, **109**, 309–318.
4 M. Farhat, H. Cox, M. Ghanem, C. M. Denkinger, C. Rodrigues, M. S. Abd El Aziz, H. Enkh-Amgalan, D. Vambe, C. Ugarte-Gil and J. Furin, *et al.*, *Nat. Rev. Microbiol.*, 2024, 1–19.
5 D. Liebenberg, B. G. Gordhan and B. D. Kana, *Front. Cell. Infect. Microbiol.*, 2022, **12**, 943545.
6 P. E. Almeida Da Silva and J. C. Palomino, *J. Antimicrob. Chemother.*, 2011, **66**, 1417–1430.
7 C. Walsh, *Nature*, 2000, **406**, 775–781.
8 E. M. Darby, E. Trampari, P. Siasat, M. S. Gaya, I. Alav, M. A. Webber and J. M. Blair, *Nat. Rev. Microbiol.*, 2023, **21**, 280–295.
9 J. Bengtsson-Palme, E. Kristiansson and D. J. Larsson, *FEMS Microbiol. Rev.*, 2018, **42**, fux053.
10 M. Zhu and X. Dai, *mSphere*, 2018, **3**, 10–1128.
11 M. Szadziul, A. Goryluk-Salmonowicz and M. Popowska, *Front. Microbiol.*, 2025, **16**, 1584660.
12 Z.-C. Zhou, J. Zheng, Y.-Y. Wei, T. Chen, R. A. Dahlgren, X. Shang and H. Chen, *Environ. Sci. Pollut. Res.*, 2017, **24**, 23753–23762.
13 E. Ledger, S. Mesnage and A. Edwards, Human serum triggers antibiotic tolerance in Staphylococcus aureus, *Nat. Commun.*, 2022, **13**, 2041.
14 J. Thomas, S. Linton, L. Corum, W. Slone, T. Okel and S. L. Percival, *Int. Wound J.*, 2012, **9**, 428–435.
15 S. Swaminath, A. Paul, A. Pradhan, J. Sebastian, R. R. Nair and P. Ajitkumar, *Microbiology*, 2020, **166**, 180–198.

16 S. Majee, A. R. Chowdhury, R. Pinto, A. Chattopadhyay, A. N. Agharkar, D. Chakravortty and S. Basu, *Commun. Biol.*, 2021, **4**, 1173.
17 A. Agrawal, S. Sinha, R. Mukherjee and D. Mampallil, *Phys. Fluids*, 2020, **32**, 093308.
18 G. Zhang, J. Bai, Y. Zhai, J. Jia, Q. Zhao, W. Wang and X. Hu, *J. Adv. Res.*, 2024, **59**, 129–140.
19 G. Larrouy-Maumus, L. B. Marino, A. V. Madduri, T. Ragan, D. M. Hunt, L. Bassano, M. G. Gutierrez, D. B. Moody, F. R. Pavan and L. P. S. De Carvalho, *ACS Infect. Dis.*, 2016, **2**, 352–360.
20 S. K. Hatzios, C. E. Baer, T. R. Rustad, M. S. Siegrist, J. M. Pang, C. Ortega, T. Alber, C. Grundner, D. R. Sherman and C. R. Bertozzi, *Proc. Natl. Acad. Sci. U. S. A.*, 2013, **110**, E5069–E5077.
21 B. B. Luthuli, G. E. Purdy and F. K. Balagaddé, *PLoS One*, 2015, **10**, e0136231.
22 J. C. Conrad and R. Poling-Skutvik, *Annu. Rev. Chem. Biomol. Eng.*, 2018, **9**, 175–200.
23 R. A. Ripandelli, A. M. van Oijen and A. Robinson, *J. Phys. Chem. B*, 2024, **128**, 10311–10328.
24 N. Qin, P. Zhao, E. A. Ho, G. Xin and C. L. Ren, *ACS Sens.*, 2021, **6**, 3–21.
25 W. Postek, N. Pacocha and P. Garstecki, *Lab Chip*, 2022, **22**, 3637–3662.
26 B. B. Aldridge, M. Fernandez-Suarez, D. Heller, V. Ambravaneswaran, D. Irimia, M. Toner and S. M. Fortune, *Science*, 2012, **335**, 100–104.
27 J.-C. Palomino, A. Martin, M. Camacho, H. Guerra, J. Swings and F. Portaels, *Antimicrob. Agents Chemother.*, 2002, **46**, 2720–2722.
28 A. V. Nguyen, M. Yaghoobi, M. Azizi, M. Davaritouchaee, K. W. Simpson and A. Abbaspourrad, *Commun. Eng.*, 2023, **2**, 15.
29 O. Scheler, K. Makuch, P. R. Debski, M. Horka, A. Ruszczak, N. Pacocha, K. Sozański, O.-P. Smolander, W. Postek and P. Garstecki, *Sci. Rep.*, 2020, **10**, 3282.
30 W. Postek and P. Garstecki, *Acc. Chem. Res.*, 2022, **55**, 605–615.
31 A. Agrawal, M. Gopu, R. Mukherjee and D. Mampallil, *Langmuir*, 2022, **38**, 4567–4577.
32 Y. Wakamoto, N. Dhar, R. Chait, K. Schneider, F. Signorino-Gelo, S. Leibler and J. D. McKinney, *Science*, 2013, **339**, 91–95.
33 W. Postek, N. Pacocha and P. Garstecki, *Lab Chip*, 2022, **22**, 3637–3662.
34 I. L. Sparks, K. M. Derbyshire, W. R. Jacobs Jr and Y. S. Morita, *J. Bacteriol.*, 2023, **205**, e00337-22.
35 O. Danilchanka, M. Pavlenok and M. Niederweis, *Antimicrob. Agents Chemother.*, 2008, **52**, 3127–3134.
36 M. Balganesh, N. Dinesh, S. Sharma, S. Kuruppath, A. V. Nair and U. Sharma, *Antimicrob. Agents Chemother.*, 2012, **56**, 2643–2651.
37 M. Laws, P. Jin and K. M. Rahman, *Trends Microbiol.*, 2022, **30**, 57–68.
38 Y. Huang, Q. Shen, H. Xu, L. Huang, S. Xiang, P. Li, L. Fan and J. Xie, *Commun. Biol.*, 2024, **7**, 1035.
39 Y. Lu, L. Wang, H. Duanmu, C. Chanyasulkit, A. J. Strong and H. Zhang, *Handbook of global tuberculosis control*, Springer, 2017.
40 S. Chen, Y. Zhou, Y. Chen and J. Gu, *Bioinformatics*, 2018, **34**, i884–i890.
41 B. Langmead and S. L. Salzberg, *Nat. Methods*, 2012, **9**, 357–359.
42 A. Dobin, C. A. Davis, F. Schlesinger, J. Drenkow, C. Zaleski, S. Jha, P. Batut, M. Chaisson and T. R. Gingeras, *Bioinformatics*, 2013, **29**, 15–21.
43 Y. Liao, G. K. Smyth and W. Shi, *Bioinformatics*, 2014, **30**, 923–930.
44 M. I. Love, W. Huber and S. Anders, *Genome Biol.*, 2014, **15**, 1–21.
45 J. W. Pylvänäinen, R. F. Laine, B. M. Saraiva, S. Ghimire, G. Follain, R. Henriques and G. Jacquemet, *J. Cell Sci.*, 2023, **136**, jcs260728.
46 F. Padovani, B. Mairhörmann, P. Falter-Braun, J. Lengefeld and K. M. Schmoller, *BMC Biol.*, 2022, **20**, 174.
47 K. J. Cutler, C. Stringer, T. W. Lo, L. Rappez, N. Stroustrup, S. Brook Peterson, P. A. Wiggins and J. D. Mougous, *Nat. Methods*, 2022, **19**, 1438–1448.
48 K. M. Rath, A. Maheshwari, P. Bengtson and J. Rousk, *Appl. Environ. Microbiol.*, 2016, **82**, 2012–2020.
49 F. Li, X.-S. Xiong, Y.-Y. Yang, J.-J. Wang, M.-M. Wang, J.-W. Tang, Q.-H. Liu, L. Wang and B. Gu, *Front. Microbiol.*, 2021, **12**, 705326.
50 M. Gopu and D. Mampallil, *Phys. Fluids*, 2022, **34**, 102110.
51 S. Vijay, M. Nagaraja, J. Sebastian and P. Ajitkumar, *Arch. Microbiol.*, 2014, **196**, 157–168.
52 K. Schubert, B. Sieger, F. Meyer, G. Giacomelli, K. Böhm, A. Rieblinger, L. Lindenthal, N. Sachs, G. Wanner and M. Bramkamp, *mBio*, 2017, **8**, 10–1128.
53 F. Bardou, A. Quemard, M.-A. Dupont, C. Horn, G. Marchal and M. Daffé, *Antimicrob. Agents Chemother.*, 1996, **40**, 2459–2467.
54 S. Mohamad, P. Ibrahim and H. A. Wahab, *Chemotherapy*, 2007, **53**, 263–266.
55 E. G. Salina, B. A. Martini, V. V. Sorokin and A. L. Mulyukin, *Front. Microbiol.*, 2024, **15**, 1494147.
56 S. N. Goossens, S. L. Sampson and A. Van Rie, *Clin. Microbiol. Rev.*, 2020, **34**, 10–1128.
57 Ž. Maglica, E. Özdemir and J. D. McKinney, *mBio*, 2015, **6**, DOI: 10.1128/mbio.02236-14.
58 G. Manina, A. Griego, L. K. Singh, J. D. McKinney and N. Dhar, *EMBO J.*, 2019, **38**, e101876.
59 J. J. Lee, S.-K. Lee, N. Song, T. O. Nathan, B. M. Swarts, S.-Y. Eum, S. Ehrt, S.-N. Cho and H. Eoh, *Nat. Commun.*, 2019, **10**, 2928.
60 K. N. Adams, K. Takaki, L. E. Connolly, H. Wiedenhoft, K. Winglee, O. Humbert, P. H. Edelstein, C. L. Cosma and L. Ramakrishnan, *Cell*, 2011, **145**, 39–53.
61 C. Chen, S. Gardete, R. S. Jansen, A. Shetty, T. Dick, K. Y. Rhee and V. Dartois, *Antimicrob. Agents Chemother.*, 2018, **62**, 10–1128.
62 L. Amaral and M. Viveiros, *Antibiotics*, 2017, **6**, 3.
63 C. E. Krämer, A. Singh, S. Helfrich, A. Grünberger, W. Wiechert, K. Nöh and D. Kohlheyer, *PLoS One*, 2015, **10**, e0141768.

64 T. F. Byrd IV, L. Hoang, E. Kim, M. Pfister, E. Werner and S. Arndt, *et al.*, The microfluidic multitrap nanophysiometer for hematologic cancer cell characterization reveals temporal sensitivity of the calcein-AM efflux assay, *Sci. Rep.*, 2014, **4**, 5117–5117.
65 A. Palande, S. Patil, A. Veeram, S. S. Sahoo, T. Lodhiya, P. Maurya, B. Muralikrishnan, J. Chugh and R. Mukherjee, *ACS Infect. Dis.*, 2024, **10**, 890–906.
66 J. Lin, D. Zhou, T. A. Steitz, Y. S. Polikanov and M. G. Gagnon, *Annu. Rev. Biochem.*, 2018, **87**, 451–478.
67 P. E. A. da Silva, A. Von Groll, A. Martin and J. C. Palomino, *FEMS Immunol. Med. Microbiol.*, 2011, **63**, 1–9.
68 S. Remm, J. C. Earp, T. Dick, V. Dartois and M. A. Seeger, *FEMS Microbiol. Rev.*, 2022, **46**, fuab050.
69 M. D. Rolfe, C. J. Rice, S. Lucchini, C. Pin, A. Thompson, A. D. Cameron, M. Alston, M. F. Stringer, R. P. Betts and J. Baranyi, *et al.*, *J. Bacteriol.*, 2012, **194**, 686–701.
70 S. Mishra, P. R. Singh, X. Hu, L. Lopez-Quezada, A. Jinich, R. Jahn, L. Geurts, N. Shen, M. A. DeJesus and T. Hartman, *et al.*, *Proc. Natl. Acad. Sci. U. S. A.*, 2025, **122**, e2425981122.